Wireless Communication in Modular Multilevel Converters and Electromagnetic Interference Characterization

Barış Çiftçi, Tim Augustin, James Gross, Staffan Norrga, and Hans-Peter Nee

***Abstract*—Recently, the wireless control of modular multilevel converter (MMC) submodules was proposed. The success of the control depends on specialized control methods suitable for wireless communication and a properly designed wireless communication network in the MMC hall. The wireless communication in the hall can be affected by the electromagnetic interference (EMI) of voltage and current transients in the converter hall. In this article, firstly, a wireless communication network design based on 5G New Radio is exemplified for an industrial size MMC. Then radiated EMI characteristics of MMC submodules with different voltage and current ratings and two dc circuit breakers are measured. The effects of interference on wireless communication in the multi-GHz frequency band are tested. The interference from the components is confined below 500 MHz, and the wireless communication with 5825 MHz center frequency is not affected by the interference.**

***Index Terms*—Circuit breakers, electromagnetic interference, multilevel converters, wireless communication.**

I. Introduction

THE modular multilevel converter (MMC) is extensively used in high-voltage multi-megawatt applications such as high-voltage dc (HVdc) transmission systems [1]. The communication between the MMC central controller and the submodules are realized by optical fiber cables conventionally as they are immune to electromagnetic interference (EMI) and provide galvanic isolation between the connecting entities [2] [1]. On the other hand, the total number of MMC submodules to reach the targeted power ratings might be in the range of thousands [3], and the dimensions of MMC valve halls might rise to hundreds of meters [4] for HVdc transmission applications. Then, below are the challenges with the use of optical fiber cables in such a big MMC valve hall [2]:

1) Laying out, terminating, and insulation testing thousands of fiber cables with hundreds of meters in length requires significant workforce and time during the installation of the MMC. Moreover, each cable needs to be identified and checked whether it connects the correct terminals during the commissioning of the MMC, which further increases the numbers [5]. The required workforce and time for all these processes contribute to the initial cost of the MMC station, with several other factors mostly specific to the project. Examples of voltage-sourced converter overall costs in HVdc transmission applications, which are considered to be mainly MMCs, are available in the literature[3]. The cost of converter station per MW ranges from 218 €k/MW to 429 €k/MW in [6] for eight different projects with power ratings from 700 MW to 3000 MW. Cigre exemplifies the converter cost as 102 €k/MW and 220 €k/MW for two projects with 1500 MW and 1000 MW ratings [7]. The share of fiber-cable-related costs in the overall costs of an MMC station is not publicly available to the authors' best knowledge. On the other hand, typical commissioning and erection costs for a new HVdc facility are estimated as 8 % of the overall costs in [8], but the elements of the mentioned costs are not provided[4].
2) The routing of the thick cable bundles in the MMC valve hall can be cumbersome and requires a resource-intensive mechanical design process during the project development process[5].
3) With thousands of submodules and hundreds of meter valve hall dimensions, the total length of optical fiber cables in an MMC valve hall is in the range of tens of kilometers[6]. Then[7], these cables lead to an increase in the converter footprint, weight, and volume, which are issues especially in off-shore and in-city transmission platforms [9].
4) The cable bundles might complicate the removal and replacement of the (failed) submodules during the maintenance of the MMC, thus increasing the maintenance time.
5) The fiber cables present an insulation breakdown risk between the central controller (low-voltage area) and the submodules (high-voltage area) due to, e.g., accumulation of dust and humidity on them.
6) The fiber cables risk spreading fire in the MMC valve hall [10]. To minimize the risks, cables made from special material and with coatings are to be used, such as

B. Çiftçi, T. Augustin, J. Gross, S. Norrga, and H.-P. Nee are with KTH Royal Institute of Technology, SE-100 44 Stockholm, Sweden (e-mail: bacif@kth.se; timau@kth.se jamesgr@kth.se; norrga@kth.se; hansi@kth.se).

[1] Well, cables are also much more reliable than wireless, which is perhaps the main reason XXX

[2] Better: Therefore, substantial challenges arise from such a cable-based deployment regarding big MMC valve halls

[3] I assume you refer here to the following values. Better to use a colon then ...

[4] Better: while the exact cost structure is unclear

[5] phase?

[6] shouldn't that be more? For instance, an A380 carries 800 km of cables in it, and is for sure smaller in dimensions ....

[7] You have a pattern of using "then" in a specific way. Be carefully with that, it is ok but not natural. Try to eliminate/substitute the thens as much as possible ...

flame-retardant, non-combustible, or self-extinguishing, which increase the cost and might complicate the layout of the bundles due to their poorer mechanical properties.

7) The fiber cables might be subject to mechanical stress and fatigue, which leads to failure. The share of *Control and Protection* systems, including *Control and Protection Telecommunications* subsystem, in the Forced Energy Unavailability (FEU) hours of the HVdc systems worldwide is 7.8 % between years 1983-2016 and 7.1 % between years 2017-2018. The other two subsystems included in the figure are *Local Control and Protection*, and *Master Control and Protection* subsystems [11].

Wireless control of MMC submodules was proposed in [12], implemented and verified in [13] to solve the challenges mentioned above. The verification of the proposal in [13] is based on using a laboratory-scale single-phase MMC with three half-bridge submodules per arm. The experimental setup does not represent an industrial-scale MMC and its valve hall in terms of the dimensions, number of communication nodes, and electrical characteristics. If the radiated electromagnetic interference (EMI) from the MMC components coincides with the wireless transmission frequency, higher transmission errors can be expected, which might complicate the wireless control of the submodules. Also, high-power transients resulting from, e.g., electrical arcs and circuit breaker operations can interfere with communication [14], [15].

The steady-state operation of industrial-scale MMCs, which mainly represents the switching of the semiconductors in the submodules, is observed to generate interference up to $1.4\,\mathrm{GHz}$, but have significant effects up to $400\,\mathrm{MHz}$ in and out of the MMC hall [16], [17]. In another study, the interference in the MMC hall is measured up to $600\,\mathrm{MHz}$ [18].

This article aims firstly to provide a more realistic wireless network design for an industrial-scale MMC. A [8] case study is carried out on an example MMC used in HVdc transmission. The second goal of the article is to present a more realistic EMI environment of an industrial-scale MMC submodule compared to that in [13] and observe its effects, if any, on wireless communication. For this aim, firstly, the radiated EMI (henceforth called just EMI) of two different laboratory-scale submodules are measured with various dc-side voltage and ac-side current levels. Then, the EMI of two different dc circuit breakers (DCCBs) are measured with $1\,\mathrm{kA}$ peak interrupted current. Lastly, wireless communication packet-loss characteristics are measured in the close vicinity of a selected submodule to observe if the EMI from the submodule affects the communication.

The structure of the article is as follows. In Section II, the wireless network design is exemplified for an industrial-scale MMC valve hall. In Section III, the EMI spectrum of MMC components is analyzed in a laboratory environment. Section IV contains wireless communication packet loss characteristics comparison when an MMC submodule operates nearby and not. Conclusions are given in Section V.

[8]theoretical?

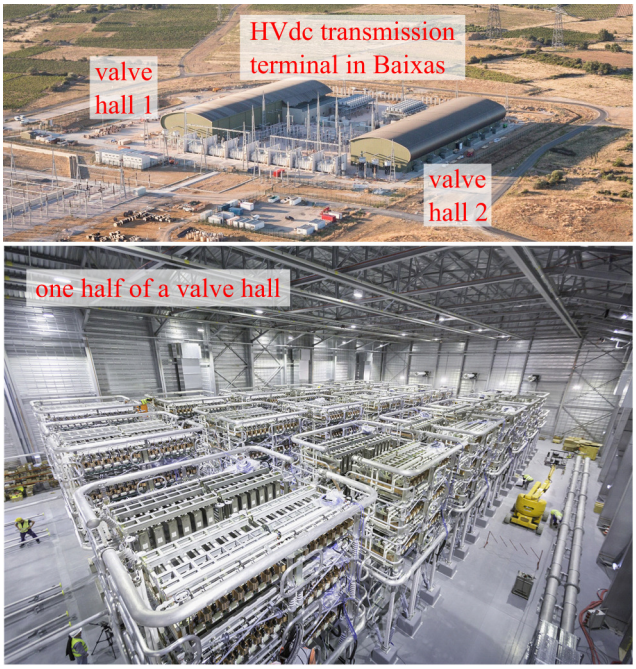

Fig. 1. MMC valve halls in Baixas[11] (a) outside (b) inside.

II. Wireless Network Design Case Study in an MMC Valve Hall

In this subsection, a wireless network design process is exemplified for an industrial size MMC. The MMC stations used in the HVdc electrical interconnection project between Baixas (France) and Santa Llogaia (Spain) are chosen as the example application to design the wireless network for [4]. The outside and inside views of the MMC station valve hall in Baixas are shown in Fig. 1. Considering other photos of the halls, the hall building looks like a big Faraday cage that attenuates the electromagnetic interference from outside to the valve hall and vice versa. Each MMC comprises of roughly 2600 half-bridge submodules in thirty-six valve towers, as shown in Fig. 1 [3]. The other parameters of the application to exemplify the wireless network is shown in Table I [9]. It is important to note that the transmission cycle, wireless payload, packet error rate, and end-to-end latency limit do not represent the parameters in the current control system of the MMC in Fig. 1. They are all taken from the parameters of the laboratory-scale wireless control implementations in [13] and [19], with the exception that 70 % of the wireless payload in Table I is spare compared to the specified implementations. Hence, the parameters in Table I correspond to a fictitious MMC. The transmission cycle and the wireless payload in Table I result in a $5.12\,\mathrm{Mb}ps$ raw data rate. [10]

[9]Could you split the table into two separate ones, and in the presentation/discussion of this entire subsection distinguish between "plant dimension" and "application requirements"? Using these two expressions should make it more clear what you are after in this part.

[10]To understand this, I need somewhere the information who transmits to whom - can you make a drawing or so to illustrate this? It becomes important later, as you want to explain to the reader how many antennas are to be reached, and how many base stations you need for this. It is also important in this context of you are interested in uplink or downlink ....

TABLE I
WIRELESS COMMUNICATION APPLICATION PARAMETERS

Parameter	Value
Valve hall dimensions (approximately)	$114\,\mathrm{m} \times 33\,\mathrm{m} \times 16\,\mathrm{m}$ [20]
Number of receiver nodes	2592 [3]
Transmission cycle (broadcast, unidirect.)	$100\,\mu\mathrm{s}$ [13]
Wireless payload (excluding any header)	64 B [13]
Packet error rate at the application layer	10^{-2} – 10^{-3} [19]
End-to-end latency limit	$200\,\mu\mathrm{s}$ [13]

A. Wireless Network in the Valve Hall

MMC submodules control is a time-critical process. It requires low end-to-end latency and high reliability in the control system. The typical sampling period in the control system of the MMCs (and similar power electronics applications) is in the range of $100\,\mu\mathrm{s}$ [13]. The application layer packet error rate (PER) requirement for the power electronics applications is in the 1×10^{-8}–1×10^{-9} range in [21] [12]. Using the control method in [19] [13], increasing the suitable PER value up to 1×10^{-2}–1×10^{-3} range is possible. In any case, the low-latency, high-reliability wireless communication solutions can be exploited for the targeted wireless control system. In this sense, 5G New Radio (NR), which is standardized with 5G release 15 [14], is a promising ultra-reliable low-latency communication solution [22], [23].

5G NR operates in frequency bands in two frequency ranges: Frequency Range 1 (FR1) for bands within $410\,\mathrm{MHz}$ to $7125\,\mathrm{MHz}$, and Frequency Range 2 (FR2) for bands within $24\,250\,\mathrm{MHz}$ to $52\,600\,\mathrm{MHz}$ [24]. 5G has a frame structure of $10\,\mathrm{ms}$ long in the physical layer. Each frame comprises ten sub-frames with a $1\,\mathrm{ms}$ length, and each sub-frame is made up of scalable transmission time intervals (TTIs). One or more consecutive slots allocated to either downlink (DL) or uplink (UL) make up a TTI. Each slot contains 14 OFDM symbols, and the length of each slot can be in the range of $62.5\,\mu\mathrm{s}$ to $1\,\mathrm{ms}$. The length of the slot depends on the employed sub-carrier spacing (SCS) frequency which is $15\,\mathrm{kHz}$, $30\,\mathrm{kHz}$, or $60\,\mathrm{kHz}$ for FR1 operation and $60\,\mathrm{kHz}$, $120\,\mathrm{kHz}$, or $240\,\mathrm{kHz}$ for FR2 operation. In 5G release 16, the maximum SCS frequency used for data transmission is $120\,\mathrm{kHz}$ in FR2, and the corresponding slot duration is $125\,\mu\mathrm{s}$. Hence, the shortest achievable slot duration for data transmission with the full slot structure with 14 OFDM symbols is $125\,\mu\mathrm{s}$. On the other hand, 5G NR introduces mini-slot transmissions with 2, 4, or 7 OFDM symbols in the DL and 1 or any more integer number of OFDM symbols in the UL. [15] Considering that OFDM symbol duration is $8.92\,\mu\mathrm{s}$ with SCS equal to $120\,\mathrm{kHz}$, using mini-slot transmission consisting of 2 OFDM symbols, the shortest achievable slot duration for data transmission can be lowered to $18\,\mu\mathrm{s}$ in the DL. Correspondingly, this is the minimum slot duration that the central controller can employ to broadcast the required data to the submodules in the MMC. Data processing time in the central and submodule controllers is added onto the slot duration and forms the end-to-end latency altogether. It is plain [16] that the exact end-to-end latency depends on the specific application, but the target transmission cycle of $100\,\mu\mathrm{s}$ seems like an achievable target even with some re-transmission to increase the reliability of the communication.

B. Antenna Placement in the Valve Hall

The wireless communication eliminates all the workload and costs related to laying out, terminating, and testing the optical-fiber cables. On the other hand, the placement of the antennas for the central controller and the submodules is introduced as a new task. In the valve hall, an enclosure around the submodule control units while the chassis is connected to the earth is common to provide electromagnetic immunity from nearby interference sources. If the wireless communication antennas of the submodules are placed inside the enclosure, the received radio power will be attenuated by the enclosure depending on the enclosure material and thickness. The authors [17] propose that the antennas be placed out of the enclosures to avoid attenuation by the enclosure. The antenna placement, the type of antenna to use, connections between the antenna and the transceiver circuitry require a comprehensive engineering study to minimize the packet error rate and not to present any threat to electrical safety. The critical points to consider for the antenna placement are listed as below:

1) The antenna placement should maximize the received radio power considering the other constraints. A direct line-of-sight is desirable.
2) The propagation environment is complex to model in a valve hall with all the conductive elements and metal bars. The assessment of the antenna placement would require detailed design, simulations, and various tests in the valve hall considering the packet error rates.
3) The antennas should not present an electrical safety risk in the high-voltage environment. Hence rod-like and pointy antennas should be avoided in the valve hall. The electric field redistribution in the valve hall should be taken into account.

Three alternative antenna placements for the submodules and the central controller are considered in this article and illustrated in Fig. 2. The alternatives are compared from

[11] https://www.windpowermonthly.com/article/1343089/gallery-france-spain-2gw-hvdc-link
https://www.ree.es/sites/all/inelfe/webscroll.html

[12] Say here that this is not reachable with current or upcoming wireless technology.

[13] This one you just give away as if it is some unimportant thing. You need to make this point much more prominent. You proposed in related work a method that can cope with the reliability levels that contemporary systems could reach ! You need to sell it to the reader here !!

[14] URLLC is release 16, and I believe that is what you base your discussions below on

[15] Here, you have a logical break. Before, you talked about 5G NR in general, while from this point on you talk about your choice of parameter setting such that the application requirements can be fullfilled. You need to explain this to the reader ...

[16] like the great plains in the west of the US?

[17] Just say we

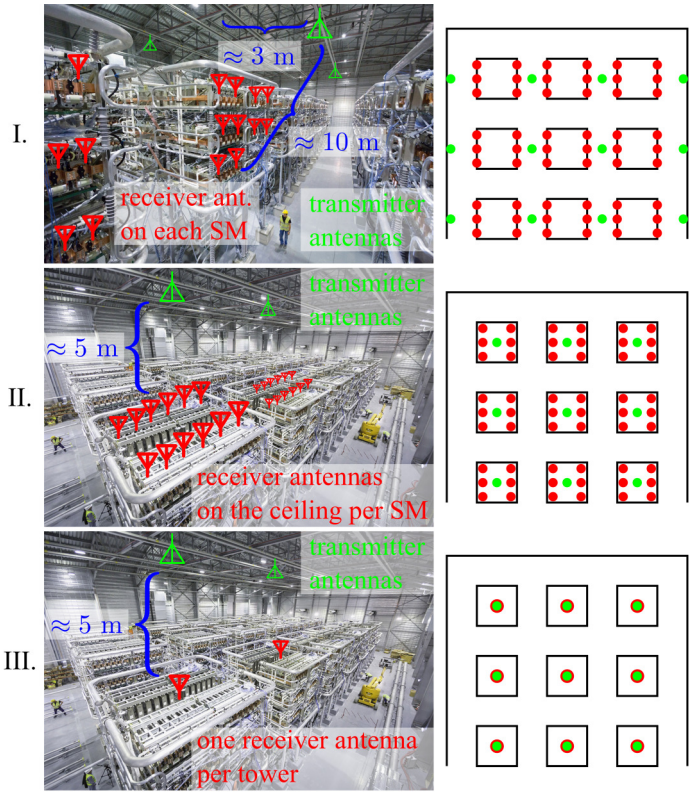

Fig. 2. Three antenna placement alternatives: (I) one (set of) antenna per submodule, within the submodule structure, (II) one (set of) antenna per submodule, away from the submodule, (III) one (set of) antenna per tower connected to all the submodules in the tower.

different perspectives as in Table II. It is considered that option III should be avoided as it presents a single point of failure in the valve tower and due to its drawbacks in terms of electrical isolation and latency. Considering options I and II, option II might have an advantage only in having a direct line-of-sight between the transmitter and all the receiver antennas and thus a better signal reception performance. As long as all the submodules can receive the wireless data well enough, option I seems like a better alternative considering the other factors. The definite choice would require detailed analysis and tests in terms of signal reception, packet error rate, and whether the errors can be compensated by other measures like autonomous submodule controllers [19]. [18]

III. EMI Spectrum Analyses of MMC Components

The EMI of two different submodules and two different DCCBs are measured in a laboratory environment. In all the measurements, the following infrastructure is shared. The electromagnetic (EM) spectrum is analyzed with a Rohde&Schwarz FSH8 spectrum analyzer. BicoLOG 5070 X biconical antenna is used to measure EMI in $50-700\,\mathrm{MHz}$ frequency range. MVG QH800 open boundary quad-ridge horn antenna is used to measure EMI in the frequency range $0.8-6\,\mathrm{GHz}$. The spectrum analyzer is set to record the maximum measured signal during the measurements, and the measurements remained for 10 minutes for the submodules.

[18]Hm, this antenna section is a bit falling from the sky. Of course, before you tell the reader about where to put the antennas, the reader needs to understand where you would put the base stations. Also how many base stations you want to install would be importan t to know, because it determines how far the signal needs to travel from transmitter to recveiver, and that determines the SNR. You need to come to some statement about the distance to cover, and if this can be expected to be line of sight, or not.

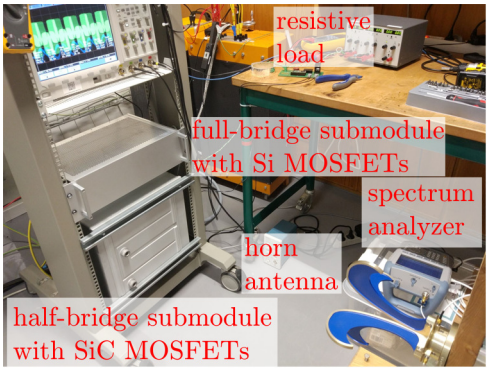

Fig. 3. Experimental setup of the submodules: full-bridge submodule with Si MOSFETs enclosed in an aluminum 19-inch rack, half-bridge submodule with SiC MOSFETs enclosed in an aluminum enclosure.

Table III shows the dynamic performance test ratings and rise rates of the voltage and current ($\mathrm{d}v/\mathrm{d}t$ and $\mathrm{d}i/\mathrm{d}t$) for the state-of-the-art semiconductors used in high-power applications. The current and voltage rise rates are calculated using the rise and fall times of the current, respectively [25]. It is considered that the table gives the correct order of magnitude for the rates, even if not the correct values, in industrial-scale MMCs.

A. Full-Bridge Submodule with Si MOSFETs

The experimental setup is shown in Fig. 3. The full-bridge submodule comprises IRFP4768PbF silicon MOSFETs (the same MOSFETs used in the experimental study in [13]) and two parallel-connected $30\,\mu\mathrm{F}$ film capacitors on the dc-side. The submodule electrical circuit and the controller are assembled on a single printed circuit board. The controller is based on the Xilinx Zynq-7000 system-on-chip. The submodule is connected to a voltage source on the dc-side by a twisted pair of cables. The ac-side is connected to variable resistors by a twisted pair of cables. Measurements are taken when the submodule is enclosed in an aluminum 19-inch rack and when not. When the submodule is enclosed, the dc- and ac-side cable pairs are shielded, and the shields are earthed on both ends. Otherwise, no shield is used. When used, the aluminum rack is earthed via the cabinet. The experiments are held with $100\,\mathrm{kHz}$ switching frequency and unipolar pulse-width modulation with 0.95 amplitude modulation index. The voltage measurements are taken directly from the MOSFET terminals. During the experiments, no other high-power equipment is operated nearby.

1) Results: Combinations of two dc-side voltages, $100\,\mathrm{V}$ and $150\,\mathrm{V}$, and four ac-side peak currents, $0\,\mathrm{A}$, $10\,\mathrm{A}$, $20\,\mathrm{A}$, and $30\,\mathrm{A}$, are experimented. The results are tagged in the figures as *volts/amperes* according to the voltage and peak current level used in the experiment. For instance, 10010 stands for the experiment run with $100\,\mathrm{V}$ dc-side voltage and $10\,\mathrm{A}$ peak ac-side current. *R-NoSw* is for the reference experiment in

TABLE II
EVALUATION OF ANTENNA PLACEMENT OPTIONS IN THE VALVE HALL

	I. One (set of) antenna per submodule, within the submodule structure	**II. One (set of) antenna per submodule, away from the submodule**	**III. One (set of) antenna per tower connected to all the submodules in the tower**
Radio signal reception	The location of the antenna is fixed within the submodule structure and has limited flexibility in terms of good signal reception. The receiver and transmitter antennas might have a line-of-sight or not.	The antennas can be placed away from the submodule (e.g., at the ceiling of the tower) for good signal reception and a line-of-sight with the transmitter antenna. Some limitations on the placement might occur due to the footprint of many antennas.	The antenna can be placed within the tower (e.g., at the ceiling of the tower) to obtain the best signal reception and a line-of-sight with the transmitter antenna.
Electrical isolation and latency	The submodule controllers are electrically isolated from each other.	The submodule controllers are electrically isolated from each other.	The single antenna output needs to be converted from electrical to, e.g., optical to provide electrical isolation between the submodule controllers and then back to electrical in the submodule controllers, adding extra latency in the control system.
Submodule assembly	The entire assembly and test of the submodule can be completed in the factory with all the communication system components installed.	The antenna connection should be done on-site and needs a cable layout within the tower. The submodules need to be tested after the antenna connections are made.	The antenna connection should be done on-site and needs a cable layout within the tower. The submodules need to be tested after the antenna connections are made.
Wireless data characteristics	Independent wireless packet losses and delay in each submodule with some correlation depending on the antenna placements.	Independent wireless packet losses and delay in each submodule with some correlation depending on the antenna placements.	The same wireless packet losses and delay in each submodule assuming the same attenuation after the reception of the signal until each submodule controller.
Maintenance of the submodule	Shorter time for submodule replacement as the antenna is a part of the submodule structure.	Longer time for submodule replacement due to the external antenna connection.	Longer time for submodule replacement due to the external antenna connection.
Cost	One (set of) antenna cost per submodule.	One (set of) antenna cost per submodule, cabling between the antenna and the submodule, laying out the cable in the tower, terminating, and commissioning after the connection.	One (set of) antenna cost per tower, cabling between the antenna to each submodule, electrical to optical converters, splitters, amplifiers, laying out the cables in the tower, terminating, commissioning after the connection.

which the converter and the controller are not energized. *R-Sw* is for the reference experiment in which the controller is energized, and the MOSFETs are switching, but the converter has 0 V dc-side voltage. The experiments with nonzero dc-side voltage are referred to as *active cases* hereafter. Fig. 4 shows the submodule ac-side voltage v_{ac} of the active cases 1000 and 1500 right after the turn-on of the respective MOSFETs that result in positive ac-side voltage. 1000 and 1500 have smooth waveforms with $\approx 0.5\,\mathrm{V/ns}$ and $\approx 0.6\,\mathrm{V/ns}$ voltage rise rates, respectively. No snubber is used for the MOSFETs.

To distinguish the EMI of different test cases, the differences in the EMI of the active cases from the reference *R-NoSw* are shown in Figs. 5 and 6 for the 150 V dc-side voltage active cases with and without the aluminum rack, respectively. The figures reveal that as soon as the switching starts in the submodule, even with zero dc-side voltage, EMI in the low-frequency range from 50 to 300 MHz is 10 to 20 dB higher

TABLE III
HIGH-POWER SEMICONDUCTORS VOLTAGE AND CURRENT RISE RATES

Device	$\mathbf{V_{cc}}$ **(V)**	$\mathbf{dv/dt}$ **(V/ns)**	$\mathbf{I_c}$ **(A)**	$\mathbf{di/dt}$ **(A/ns)**
5SNA 2000K451300[a]	2800	3.94	2000	3.02
CM1500HC-66R[b]	1800	6.00	1500	4.00
FZ1500R33HE3[c]	1800	5.14	1500	3.43

a: ABB, b: Mitsubishi Electric, c: Infineon.

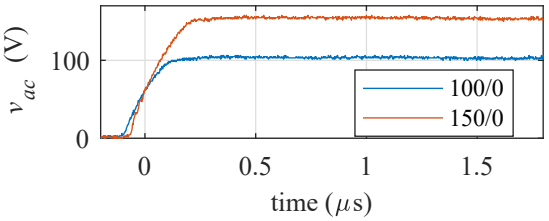

Fig. 4. Ac-side voltage waveforms of active cases 1000 and 1500 right after the turn-on of the MOSFETs that result in positive ac-side voltage.

than *R-NoSw*. Having a nonzero dc-side voltage or higher ac-side current does not affect the EMI particularly. Compared to the *R-NoSw* reference, the higher EMI is mainly related to the switchings and the driver circuit. Comparing Figs. 5.(a) and 6, the aluminum rack decreases the interference from 100 to 300 MHz up to 10 dB. In the high-frequency range, there are some outliers from 800 to 900 MHz, 2.4 to 2.7 GHz, and 5.2 to 5.6 GHz; however, no continuous frequency range has higher interference than the reference. The outliers in the $800-900$ MHz range are considered sourcing from GSM, 3G, and 4G networks, and those in 2.5 to 2.7 GHz are from 4G networks in Sweden [26]. The outliers in the 2.4 to 2.5 GHz and 5.2 to 5.6 GHz ranges are considered sourcing from the nearby WLAN networks. Consequently, the experimented full-bridge submodule does not affect the EM spectrum above

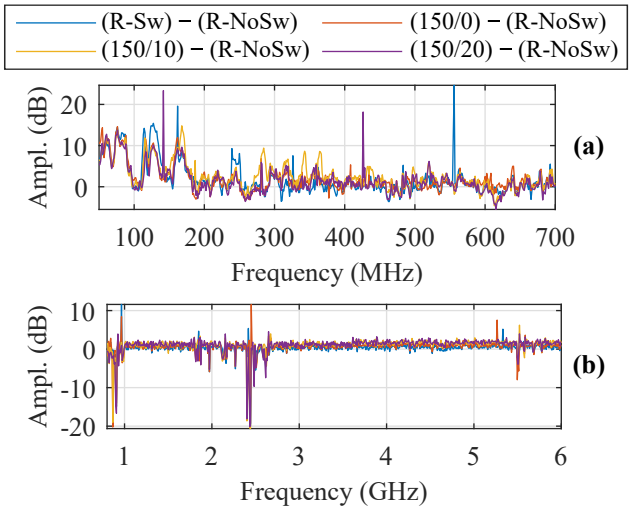

Fig. 5. EMI differences from the reference with no switching 50 to 700 MHz (a) and 0.8 to 6 GHz (b) for 150 V dc-side voltage active cases, with aluminum enclosure.

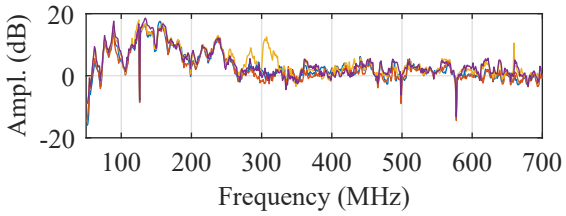

Fig. 6. EMI differences from the reference with no switching 50 to 700 MHz for 150 V dc-side voltage active cases, no aluminum enclosure. The high-frequency spectrum is similar to Fig. 5.(b). The legend of the figure is the same as in Fig. 5.

around 300 MHz. It should be remembered that the voltage rise rates in the experiments are an order of magnitude smaller than those in Table III.

B. Half-Bridge Submodule with SiC MOSFETs

The experimental setup is shown in Fig. 3. The half-bridge submodule comprises a CAS300M12BM2 half-bridge silicon-carbide MOSFET module and two parallel-connected 680 µF film capacitors. The submodule is enclosed in an aluminum enclosure. The half-bridge driver is placed in the enclosure, and it has optical fiber switching pulse inputs from the submodule controller, which is placed out of the enclosure. The controller is based on the Xilinx Zynq-7000 system-on-chip. The submodule and the controller are galvanically isolated. The submodule is connected to a voltage source on the dc-side by an unshielded twisted pair of cables. The ac-side is connected to variable resistors with a shielded pair of cables. The cable shield is earthed on both ends. The submodule enclosure is earthed via the cabinet. The experiments are held using sinusoidal pulse-width modulation with 833 Hz switching frequency and 0.95 amplitude modulation index.

1) Results: Combinations of two dc-side voltages, 200 V and 400 V, and four ac-side peak current levels, 0 A, 10 A, 20 A, and 30 A, are experimented. The results are tagged in the figures as explained in the previous subsection. Test

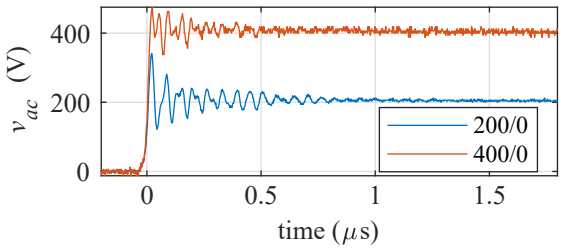

Fig. 7. Ac-side voltage waveforms of active cases 200/0 and 400/0 right after the turn-off of the low-side MOSFET.

case *R* stands for the reference in which the converter has 0 V dc-side voltage, but all the control circuits and auxiliary setup are up and running. In Fig. 7, the ac-side voltage waveform of 2000 and 4000 measurements right after the low-side MOSFET turn-off are compared. The active cases with 200 V and 400 V dc-side voltages have $\approx 14\,\mathrm{V/ns}$ and $\approx 19\,\mathrm{V/ns}$ rise rates, respectively. The values are higher than those in Table III. Oscillations in the waveforms are observed with peak-to-peak voltages of 220 V and 125 V for 2000 and 4000 active cases, respectively. The oscillations are fundamentally due to the resonant behavior of the parasitic inductance on the current path of the MOSFETs and the parasitic capacitance of the MOSFETs. The current rise rates of 20030 and 40030 active cases are 0.37 A/µs and 0.52 A/µs, respectively. They are much smaller than those in Table III. The current rise rates refer that the experimental setup has a parasitic inductance in the hundreds of µH range.

The differences in the EMI of the active cases from the reference are shown in Figs. 8 and 9 for the 200 V and 400 V dc-side voltages, respectively. The low-frequency spectra from 50 to 700 MHz present more diversity than the high-frequency spectra from 0.8 to 6 GHz in both figures. A detailed investigation reveals that most differences are individual low-bandwidth outliers in a single active case. The number and amplitudes of outliers in the 200 V cases are more than in the 400 V cases. This difference can be verified by comparing the variances of the active cases shown in the figures. The higher peak-to-peak amplitude of the switching oscillations in 200 V active cases is considered to cause more and higher amplitude EMI outliers. There are a few noticeable frequencies around which both the 200 V and 400 V cases have increased interference levels altogether by more than 5 dB. This behavior can be seen around 50 MHz and 470 MHz, but there is no relation between the increased ac-side current amplitude and the interference level. It is important to note that the LTE450 network is present at around 470 MHz [26]. In the high-frequency spectra, there are several outliers in the $800-900\,\mathrm{MHz}$ and $2.4-2.7\,\mathrm{GHz}$ ranges, and around 5.5 GHz, which are considered originating from the GSM, 3G, 4G, and WLAN networks as detailed previously. There is no consistently higher interference in all the active cases than the reference as in the low-frequency range.

The measurements are repeated with demounted submodule enclosure cover. The differences in the EMI of the active cases from the reference are shown in Fig. 10 for 400 V dc-side voltage. All the active cases have up to 20 dB higher

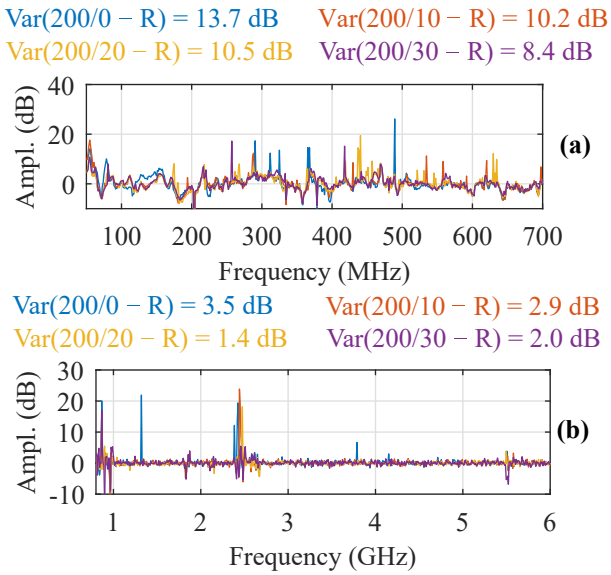

Fig. 8. EMI differences from the reference between 50 to 700 MHz (a) and 0.8 to 6 GHz (b) for 200 V dc-side voltage active cases.

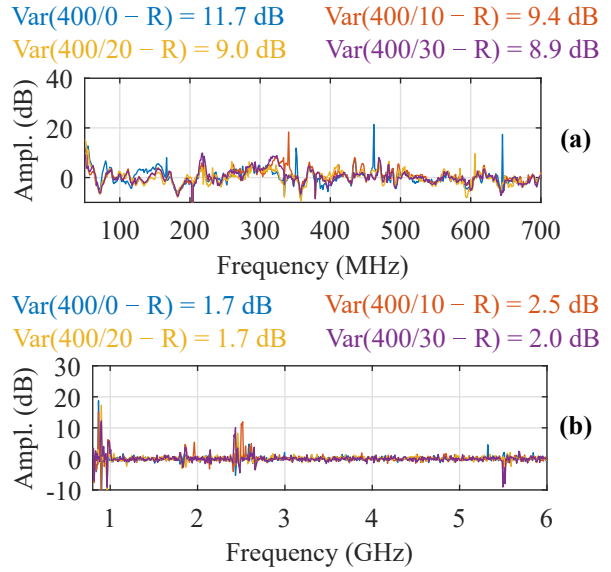

Fig. 9. EMI differences from the reference between 50 to 700 MHz (a) and 0.8 to 6 GHz (b) for 400 V dc-side voltage active cases.

interference than the reference in 50 to 350 MHz and 400 to 500 MHz ranges. The interference amplitude decreases with the frequency. When Figs. 9 and 10 are compared, the interference from the submodule is confined mostly below 500 MHz. In the high-frequency range, individual outliers are seen in the active cases in 0.8 to 1 GHz, 1.8 to 2.2 GHz, 2.4 to 2.7 GHz ranges, and around 5.5 GHz. Interference in the 1.8 to 2.2 GHz range is considered to be originating from GSM, 3G, and 4G networks [26]. The other frequency ranges were explained previously. These results are promising indications that the wireless communication in the multi-GHz frequency band would function properly with no harmful interference from the submodule switchings even without proper EM shielding.

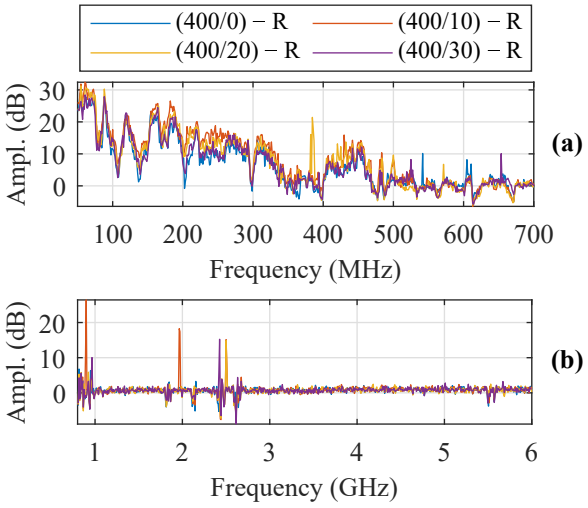

Fig. 10. EMI differences from the reference between 50 to 700 MHz (a) and 0.8 to 6 GHz (b) for 400 V dc-side voltage active cases with demounted enclosure cover.

C. DC Circuit Breakers

Because of the increased share of renewables and the move towards electrified transportation, more dc systems evolve in the electricity infrastructure that must be protected against dc-side faults. AC circuit breakers rely on the current zero-crossing of the ac fault current to interrupt. However, dc fault currents do not have a natural current zero-crossing and specialized dc circuit breakers (DCCBs) are needed to protect dc systems. A solution is the general DCCB structure depicted in Fig. 11. As shown in [27], the implementation of the general DCCB structure only affects the internal commutation processes between the parallel paths. Still, the internal commutation processes can cause different EMI throughout the operation of the DCCB because of the underlying physical phenomena and the switching transients during the commutations. Therefore, two DCCBs, which operate similarly to the two major types of DCCBs, are used in dc interruption tests: a solid-state DCCB based on an integrated gate-commutated thyristor without snubber and an enhanced active resonant (EAR) DCCB based on a triggered vacuum gap as described in [28]. As in ac circuit breakers, the core component of EAR DCCBs, the triggered vacuum gap, operates with an electric arc discharge enclosed by the device. The experimental setup is shown in Fig. 12. The current i_{dc} and voltage v_{dc} as seen by the dc system at the terminals of the DCCB measured in experiments at 1 kA are given in Fig. 13. The switching transient of v_{dc} indicates that injection-type DCCBs like the EAR DCCB commutate slower than semiconductor-based DCCBs. The maximum $\mathrm{d}i/\mathrm{d}t$ and $\mathrm{d}v/\mathrm{d}t$ observed, considering the internal currents measured, are 61.0 A/µs and 14.3 V/µs and 80.7 A/µs and 137.8 V/µs for the EAR and solid-state DCCB, respectively. The EMI differences before and after the operation of DCCBs are shown in Fig. 14. In both cases, the interference generated by the operation of the DCCBs is marginal, and it is observed that the main source of EMI is the auxiliary circuits such as switching dc power supplies.

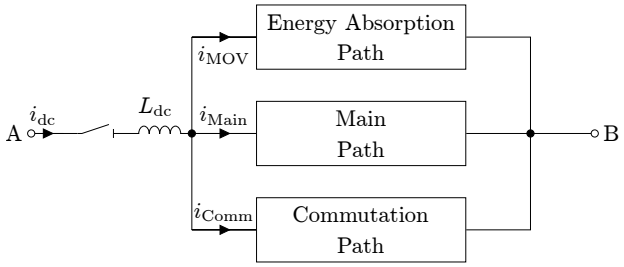

Fig. 11. General dc circuit breaker structure.

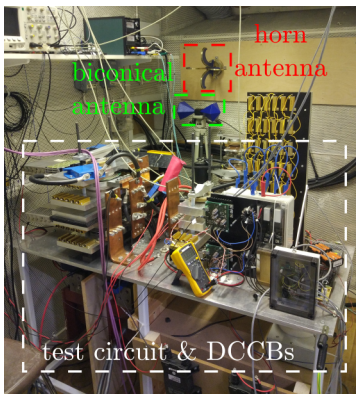

Fig. 12. Experimental setup of the solid-state and EAR DCCBs.

D. Discussion

The EMI measurements of MMC submodules with voltage rise rates up to $19\,\mathrm{V/ns}$ and current rise rates up to $0.52\,\mathrm{A/\mu s}$ resulted in the interference from the submodules being confined below $500\,\mathrm{MHz}$. The measurements with solid-state and EAR DCCBs have a marginal effect in the sub-GHz range and above. It is hypothesized that a wireless communication link with a transmission center frequency in the multi-GHz range, as proposed in Section II-A and as in [13], would not suffer from the EMI generated by the MMC submodules and DCCBs operating with similar parameters to those experimented in the previous subsections. The hypothesis will be experimented within the next section.

IV. Wireless Communication Packet Loss Characteristics

In order to verify the hypothesis raised in Section III-D, packet losses of the employed wireless communication are

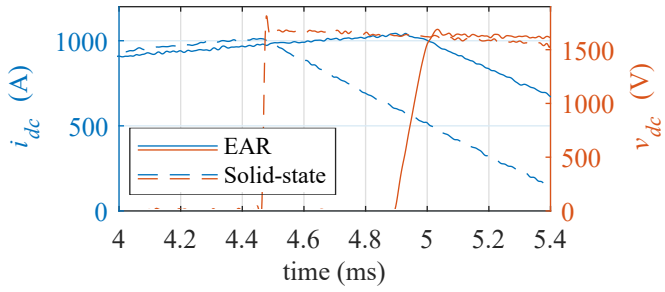

Fig. 13. The internal currents and the voltage of the DCCB measured in dc interruption tests at 1 kA.

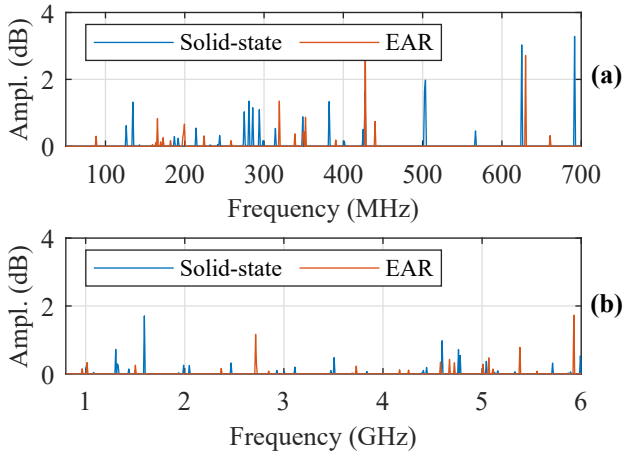

Fig. 14. The EMI differences before and after the operation of DCCBs operated at 1 kA between 50 to 700 MHz (a) and 0.8 to 6 GHz (b).

measured in the presence of the EMI generated by the specified half-bridge submodule in Section III-B, and the results are compared to a reference measurement. The measurement setup and the surrounding environment are sketched in Fig. 15. The submodule and the receiver are fixed, and the transmitter is set 2, 4, 8, and 16 m apart from the submodule in different measurement campaigns. The transceivers are in the line of sight. Several electrical motors, metal structures, frames, bench legs, and fences are in the surrounding environment. Computers, monitors, and bench-top equipment are placed on the benches and attached frames. Metal pipes are along the ceiling, and the floor material is semiconducting. Power panels with metal covers are placed on the side walls. All the surroundings present a unique EM wave propagation environment, which probably does not match an industrial-scale MMC hall. However, some resemblance can be argued with the metal frames, pipes along the ceiling, and power panels on the walls. It is considered that in an MMC hall, antenna placements with direct line-of-sight and a couple of tens of meters of distance might be realistic, as proposed by option II in Section II-B. From the electrical rating point-of-view, the voltage rise rate of the employed submodule is higher than that of the considered industrial-scale MMCs, but the current rise rate is much smaller, as expressed in Section III-B1.

The wireless transceivers are based on WARP v3 kits. WARP project offers a reference IEEE 802.11 orthogonal frequency-division multiplexing physical layer (PHY) and a distributed coordination function medium access control (MAC) design [29]. In this study, carrier-sense and random backoff mechanisms of the MAC layer are disabled, and PHY is used for wireless communication. The wireless transmitter is connected to a controller serving as the central controller of an MMC. The wireless receiver is connected to the submodule controller as in Section III-B. The submodule controller is reached remotely during the measurements to observe the number of packet losses. The measurements are conducted in a stationary environment. The employed wireless communication parameters are listed in Table IV. The transmission

TABLE IV
WIRELESS COMMUNICATION PARAMETERS

Protocol	IEEE 802.11a	Transmiss. period	100 µs
Data rate	18 Mbit/s	Transmiss. power	10 dBm
Modulation	QPSK	Transmiss. center freq.	5825 MHz
Payload	32 B	Transmiss. bandwidth	20 MHz

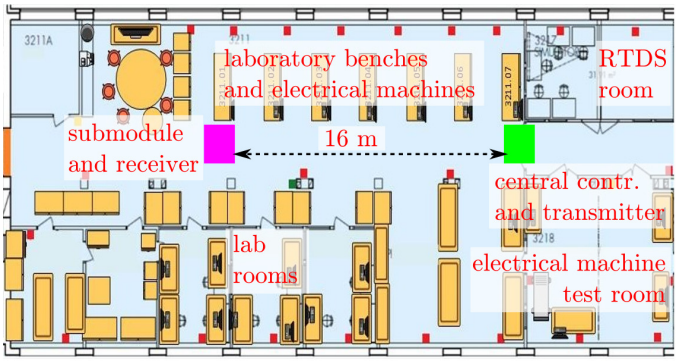

Fig. 15. The sketching of the experimental setup for wireless communication packet loss measurements and the surrounding environment.

center frequency is towards the end of the 5 GHz band, which is not affected by the EMI of experimented submodules and DCCBs. It is also less frequently occupied by other wireless devices.

The submodule is energized and de-energized for 10-minute periods in a round-robin fashion during the measurements. When energized, the active case 40010 is implemented. When de-energized, the reference *R* is repeated with the additional presence and operation of wireless transceivers. Table V shows the number of packet losses with specified lengths for each measurement campaign with 16 m distance between the wireless transmitter and receiver (the other tables corresponding to 2 , 4 , and 8 m distances are not shown for brevity). The number of packet losses for each loss length and the fraction of lost packets are similar for the 40010 and the *R* measurements in each campaign. The mean and standard deviation of the packet losses are close to each other. The packet losses are dependent on the distance between the transceivers, as expected. However, considering each campaign in itself, there is no indication that the EMI from the submodule causes more wireless packet losses. Thus, the measurement results confirm that the EMI from the submodule does not deteriorate wireless communication.

V. CONCLUSION

In this article, firstly, a wireless network design is exemplified on an industrial-size MMC used for HVdc transmission. Considering the size of the MMC valve hall, number of submodules, and parameters related to the MMC control system, the 5G NR solution seems promising to provide the required broadcast cycle. Three options for wireless antenna placements in the MMC hall are envisioned and compared in different aspects. It is considered that an antenna (set) integrated with the submodule structure might be preferential, but the definite choice requires more detailed analysis and

TABLE V
WIRELESS COMMUNICATION PACKET LOSSES, 16 m DISTANCE

Measurement	Loss length (packets)					
	1	2	3	4	5	6
	7	8	9	10	10+	FLP*
400/10-1	131497	21544	4649	1191	356	139
	41	17	8	4	2	327
R-1	109138	15325	2920	639	176	57
	18	6	2	0	0	254
400/10-2	128299	19282	3878	899	220	66
	24	9	3	1	0	306
R-2	132522	21848	4493	1129	301	94
	30	8	2	3	1	328
400/10-3	131615	21537	4462	1094	328	97
	29	13	6	0	1	325
R-3	134778	22197	4676	1081	300	95
	33	11	7	0	1	333
400/10-4	149095	26105	5638	1461	418	130
	47	23	8	1	1	379
R-4	142471	24385	5231	1307	358	104
	38	13	3	4	0	358
400/10-5	145393	24291	5112	1251	337	108
	42	21	4	6	3	362
R-5	143050	24374	5154	1335	372	83
	23	10	7	2	2	359
400/10-6	140959	23879	4985	1216	368	112
	35	16	8	1	5	353
R-6	140768	23074	4795	1166	349	130
	43	16	2	2	2	348
Mean 400/10	137810	22773	4787	1185	338	109
	36	17	6	2	2	342
Mean R	133788	21867	4545	1110	309	94
	31	11	4	2	1	330
SD† 400/10	8526	2444	603	185	66	26
	9	5	2	2	2	27
SD† R	12807	3376	844	251	72	24
	9	4	2	2	1	39

* Fraction of lost packets $(\times 10^{-4})$. 6×10^6 packets are transmitted in 10 minutes when the transmission period is 100 µs.
† Standard deviation.

tests. The second part of the article measures the EMI of two different laboratory-scale MMC submodules and DCCBs. The interference from the submodules in the steady-state operation is confined below 500 MHz. Interference from the experimented solid-state and EAR DCCBs is marginal in the whole frequency spectrum. Then, the wireless communication errors are characterized in the vicinity of the half-bridge submodule that operates with a similar voltage rise rate to an industrial-scale MMC submodule. The results verified that the generated EMI of the submodule does not interfere with the employed wireless communication with 5825 MHz transmission center frequency. This is a promising result to expect similar behavior from the industrial-scale MMC submodules. Several other points require further investigation to ensure that the EMI from the MMC components does not deteriorate wireless communication. Some of them are the submodule measurements with higher current and rise rates, the EMI from electrical arcs taking place in open space, and from shoot-through faults, i.e., a low resistance path between the submodule capacitor positive and negative terminals. Also, the placement of components in an industrial-scale MMC hall presents a unique propagation environment and should be engineered accordingly to provide proper wireless communication.

ACKNOWLEDGMENT

The authors would like to thank Seyed Samie Mostafavi for his contributions in Section II-A and the Division of Electromagnetic Engineering in KTH Royal Institute of Technology for sharing the MVG QH800 antenna.

REFERENCES

[1] S. Debnath, J. Qin, B. Bahrani, M. Saeedifard, and P. Barbosa, "Operation, control, and applications of the modular multilevel converter: A review," *IEEE Trans. Power Electron.*, vol. 30, no. 1, pp. 37–53, Jan. 2015.

[2] H.-J. Knaak, "Modular multilevel converters and HVDC/FACTS: A success story," in *Proc. 14th Eur. Conf. Power Electron. and Appl.*, Birmingham, 2011.

[3] S. Dennetiere, S. Nguefeu, H. Saad, and J. Mahseredjian, "Modeling of modular multilevel converters for the France-Spain link," in *Int. Conf. Power Syst. Transients*, Vancouver, BC, 2013.

[4] Inelfe, *Electrical interconnection between Baixas - Santa Llogaia*, (accessed Nov. 1, 2021). [Online]. Available: https://www.inelfe.eu/en/projects/baixas-santa-llogaia

[5] L. Brand et al., "Testing and commissioning of VSC HVDC systems," Cigre, Technical Brochure 697, Aug. 2017.

[6] M. Daby, "Consultancy support for Ofgem's cost assessment of the proposed NSL interconnector," Atkins, Tech. Rep., Apr. 2016.

[7] D. Westermann et al., "Voltage source converter (VSC) HVDC for power transmission – economic aspects and comparison with other AC and DC technologies," Cigre, Technical Brochure 492, Apr. 2012.

[8] R. Johnson and G. Wolf, "Refurbish rather than replace: Resuscitating aging HVdc and FACTS projects," *IEEE Power and Energy Mag.*, vol. 14, no. 2, pp. 22–31, Mar.-Apr. 2016.

[9] T. J. Stott and P. R. Couch, "Optical communications network for high voltage direct current power transmission," French Patent WO2 013 178 249Al, Dec. 5, 2013.

[10] J. Allaire et al., "Fire aspects of HVDC thyristor valves and valve halls," Cigre, Technical Brochure 136, Feb. 1999.

[11] M. Bennett and L. Crowe, "A survey of the reliability of HVDC systems throughout the world during 2017-2018," in *Cigre 2020 e-Session*, no. B4-139, Paris, 2020, pp. 1–13.

[12] B. Ciftci, J. Gross, S. Norrga, L. Kildehøj, and H.-P. Nee, "A proposal for wireless control of submodules in modular multilevel converters," in *20th Eur. Conf. Power Electron. and Appl.*, Riga, Sept. 2018, pp. 1–10.

[13] B. Çiftçi, S. Schiessl, J. Gross, L. Harnefors, S. Norrga, and H.-P. Nee, "Wireless control of modular multilevel converter submodules," *IEEE Trans. Power Electron.*, vol. 36, no. 7, pp. 8439–8453, Jul. 2021.

[14] A. Abdrabou and A. M. Gaouda, "Uninterrupted wireless data transfer for smart grids in the presence of high power transients," *IEEE Syst. J.*, vol. 9, no. 2, pp. 567–577, Jun. 2015.

[15] C. Klünder and J. Luiken ter Haseborg, "Effects of high-power and transient disturbances on wireless communication systems operating inside the 2.4 GHz ISM band," in *IEEE Int. Symp. Electromagn. Compat.*, Fort Lauderdale, FL, USA, Jul. 2010, pp. 359–363.

[16] J. Zhang, T. Lu, W. Zhang, H. Shen, and Z. Yang, "Frequency-time domain characteristics of radiated electric fields in a multi-terminal MMC-HVDC station," *IEEE Access*, vol. 7, pp. 99 937–99 944, 2019.

[17] J. Zhang, T. Lu, W. Zhang, J. Xu, and W. Li, "Measurement and analysis of radiated disturbance characteristics of ±320 kV modular multilevel converter system," *IEEE Access*, vol. 7, pp. 10 028–10 036, 2019.

[18] W. Chen, L. Jia, L. Yu, and M. Li, "Measurement and analysis of electromagnetic disturbances in 500kV dc converter station," in *China Int. Conf. Electricity Distribution*, Shanghai, Sept. 2012, pp. 1–5.

[19] B. Çiftçi, L. Harnefors, X. Wang, J. Gross, S. Norrga, and H.-P. Nee, "Wireless control of modular multilevel converter submodules with communication errors," *IEEE Trans. Ind. Electron.*, 2021, early access.

[20] *Station De Conversion HVDC Baixas*, Google Maps, (accessed Nov. 1, 2021). [Online]. Available: https://www.google.com/maps/@42.7311046,2.8012399,261m/data=!3m1!1e3

[21] M. Luvisotto, Z. Pang, and D. Dzung, "Ultra high performance wireless control for critical applications: Challenges and directions," *IEEE Trans. Ind. Informat.*, vol. 13, no. 3, pp. 1448–1459, Jun. 2017.

[22] "5G for connected industries and automation," 5G Alliance for Connected Industries and Automation, White Paper, Feb. 2019.

[23] X. Jiang, M. Luvisotto, Z. Pang, and C. Fischione, "Reliable minimum cycle time of 5G NR based on data-driven channel characterization," *IEEE Trans. Ind. Informat.*, vol. 17, no. 11, pp. 7401–7411, Nov. 2021.

[24] Devopedia, "5G NR PHY," (accessed Nov. 09, 2021). [Online]. Available: https://devopedia.org/5g-nr-phy

[25] *Application Note 5SYA 2053-04*, ABB, Sept. 2013.

[26] The Swedish Post and Telecom Authority, *Frequency band for block state*, (in Swedish), (accessed Jun. 20, 2021). [Online]. Available: https://www.pts.se/sv/bransch/radio/blocktillstand/

[27] T. Augustin, S. Norrga, and H.-P. Nee, "Modelling of HVDC breakers for HVDC grid simulations," in *13th IET Int. Conf. AC and DC Power Transmiss.*, Manchester, 2017, pp. 1–6.

[28] T. Augustin, M. Becerra, and H.-P. Nee, "Enhanced active resonant dc circuit breakers based on discharge closing switches," *IEEE Trans. Power Del.*, vol. 36, no. 3, pp. 1735–1743, Jun. 2021.

[29] *802.11 Reference Design for WARP v3*, Edgewall Software, (accessed Jun. 25, 2021). [Online]. Available: https://warpproject.org/trac/wiki/802.11